2016-10-01

Temporal multiplexing with adaptive optics for simultaneous vision.

Papadatou, E

10.1364/BOE.7.004102
Biomed Opt Express

Research Article | Vol. 7, No. 10 | 1 Oct 2016 | BIOMEDICAL OPTICS EXPRESS 4102
Biomedical Optics EXPRESS

Temporal multiplexing with adaptive optics for simultaneous vision

ELENI PAPADATOU,[1] ANTONIO J. DEL ÁGUILA-CARRASCO,[1] IVÁN MARÍN-FRANCH,[1,2] NORBERTO LÓPEZ-GIL[2,*]

[1]*Optometry Research Group, Facultad de Física, Universidad de Valencia, Spain*
[2]*CiViUM Research Group, Facultad de Óptica y Optometría, Universidad de Murcia, Spain*
[*]*norberto@um.es*

Abstract: We present and test a methodology for generating simultaneous vision with a deformable mirror that changed shape at 50 Hz between two vergences: 0 D (far vision) and −2.5 D (near vision). Different bifocal designs, including toric and combinations of spherical aberration, were simulated and assessed objectively. We found that typical corneal aberrations of a 60-year-old subject changes the shape of objective through-focus curves of a perfect bifocal lens. This methodology can be used to investigate subjective visual performance for different multifocal contact or intraocular lens designs.

OCIS codes: (330.7335) Visual optics, refractive surgery; (110.3000) Image quality assessment; (220.1010) Aberrations (global); (220.1080) Active or adaptive optics; (330.7327) Visual optics, ophthalmic instrumentation.

References and links

1. W. N. Charman, "Developments in the correction of presbyopia I: spectacle and contact lenses," Ophthalmic Physiol. Opt. **34**(1), 8–29 (2014).
2. A. Duane, "An attempt to determine the normal range of accommodation at various ages, being a revision of Donder's experiments," Trans. Am. Ophthalmol. Soc. **11**(Pt 3), 634–641 (1908).
3. I. K. O. K. Kragha, "Amplitude of Accommodation: Population and Methodological Differences," Ophthalmic Physiol. Opt. **6**(1), 75–80 (1986).
4. W. N. Charman, "Developments in the correction of presbyopia II: surgical approaches," Ophthalmic Physiol. Opt. **34**(4), 397–426 (2014).
5. E. S. Bennett, "Contact lens correction of presbyopia," Clin. Exp. Optom. **91**(3), 265–278 (2008).
6. J. A. Davison and M. J. Simpson, "History and development of the apodized diffractive intraocular lens," J. Cataract Refract. Surg. **32**(5), 849–858 (2006).
7. D. Alais and R. Blake, eds., *Binocular Rivalry* (MIT Press, 2005).
8. H. B. Dick, F. Krummenauer, O. Schwenn, R. Krist, and N. Pfeiffer, "Objective and subjective evaluation of photic phenomena after monofocal and multifocal intraocular lens implantation," Ophthalmology **106**(10), 1878–1886 (1999).
9. D. Miller and L. Meshel, "Annular mask contact lenses," U.S. patent US5245367 A (September 14, 1993).
10. G. O. Waring 4th, "Correction of presbyopia with a small aperture corneal inlay," J. Refract. Surg. **27**(11), 842–845 (2011).
11. D. A. Atchison, S. Blazaki, M. Suheimat, S. Plainis, and W. N. Charman, "Do small-aperture presbyopic corrections influence the visual field?" Ophthalmic Physiol. Opt. **36**(1), 51–59 (2016).
12. H. S. Ong, J. R. Evans, and B. D. S. Allan, "Accommodative intraocular lens versus standard monofocal intraocular lens implantation in cataract surgery," Cochrane Database Syst. Rev. **5**, CD009667 (2014).
13. M. Kalloniatis and C. Luu, "Temporal Resolution," in *Webvision: The Organization of the Retina and Visual System*, H. Kolb, E. Fernandez, and R. Nelson, eds. (University of Utah Health Sciences Center, 1995).
14. F. Scharnowski, F. Hermens, and M. H. Herzog, "Bloch's law and the dynamics of feature fusion," Vision Res. **47**(18), 2444–2452 (2007).
15. J. A. Roufs, "Dynamic properties of vision. I. Experimental relationships between flicker and flash thresholds," Vision Res. **12**(2), 261–278 (1972).
16. M. Blum, M. Büeler, C. Grätzel, J. Giger, and M. Aschwanden, "Optotune focus tunable lenses and laser speckle reduction based on electroactive polymers," in H. Schenk, W. Piyawattanametha, and W. Noell, eds. (2012), p. 825207.
17. C. Dorronsoro Díaz, J. R. Alonso Sanz, and S. Marcos Celestino, "Miniature Simultaneous Vision Simulator Instrument," U.S. patent WO/2015/049402 (April 10, 2015).
18. R. A. Applegate, E. J. Sarver, and V. Khemsara, "Are all aberrations equal?" J. Refract. Surg. **18**(5), S556–S562 (2002).
19. A. Roorda, "Adaptive optics for studying visual function: a comprehensive review," J. Vis. **11**(5), 6 (2011).

#269785 http://dx.doi.org/10.1364/BOE.7.004102
Journal © 2016 Received 5 Jul 2016; revised 17 Aug 2016; accepted 19 Aug 2016; published 15 Sep 2016

Biomedical Optics EXPRESS

20. J. L. Alió, B. Elkady, D. Ortiz, and G. Bernabeu, "Clinical outcomes and intraocular optical quality of a diffractive multifocal intraocular lens with asymmetrical light distribution," J. Cataract Refract. Surg. **34**(6), 942–948 (2008).
21. A. Glasser and M. C. W. Campbell, "Presbyopia and the optical changes in the human crystalline lens with age," Vision Res. **38**(2), 209–229 (1998).
22. D. A. Atchison, "Design of aspheric intraocular lenses," Ophthalmic Physiol. Opt. **11**(2), 137–146 (1991).
23. T. Eppig, K. Scholz, A. Löffler, A. Messner, and A. Langenbucher, "Effect of decentration and tilt on the image quality of aspheric intraocular lens designs in a model eye," J. Cataract Refract. Surg. **35**(6), 1091–1100 (2009).
24. K. M. Rocha, E. S. Soriano, W. Chamon, M. R. Chalita, and W. Nosé, "Spherical Aberration and Depth of Focus in Eyes Implanted with Aspheric and Spherical Intraocular Lenses: a Prospective Randomized Study," Ophthalmology **114**(11), 2050–2054 (2007).
25. S. Marcos, S. Barbero, and I. Jiménez-Alfaro, "Optical quality and depth-of-field of eyes implanted with spherical and aspheric intraocular lenses," J. Refract. Surg. **21**(3), 223–235 (2005).
26. N. López-Gil and V. Fernández-Sánchez, "The change of spherical aberration during accommodation and its effect on the accommodation response," J. Vis. **10**(13), 12 (2010).
27. B. Antona, F. Barra, A. Barrio, A. Gutierrez, E. Piedrahita, and Y. Martin, "Comparing methods of determining addition in presbyopes," Clin. Exp. Optom. **91**(3), 313–318 (2008).
28. L. Wang and D. D. Koch, "Custom optimization of intraocular lens asphericity," J. Cataract Refract. Surg. **33**(10), 1713–1720 (2007).
29. H. E. Gollogly, D. O. Hodge, J. L. St Sauver, and J. C. Erie, "Increasing incidence of cataract surgery: population-based study," J. Cataract Refract. Surg. **39**(9), 1383–1389 (2013).
30. R. Navarro, J. J. Rozema, and M.-J. Tassignon, "Optical changes of the human cornea as a function of age," Optom. Vis. Sci. **90**(6), 587–598 (2013).
31. E. Papadatou, A. J. Del Águila-Carrasco, J. J. Esteve-Taboada, D. Madrid-Costa, and R. Montés-Micó, "Assessing the in vitro optical quality of presbyopic solutions based on the axial modulation transfer function," J. Cataract Refract. Surg. **42**(5), 780–787 (2016).
32. D. Madrid-Costa, J. Ruiz-Alcocer, T. Ferrer-Blasco, S. García-Lázaro, and R. Montés-Micó, "Optical quality differences between three multifocal intraocular lenses: bifocal low add, bifocal moderate add, and trifocal," J. Refract. Surg. **29**(11), 749–754 (2013).
33. M. J. Kim, L. Zheleznyak, S. Macrae, H. Tchah, and G. Yoon, "Objective evaluation of through-focus optical performance of presbyopia-correcting intraocular lenses using an optical bench system," J. Cataract Refract. Surg. **37**(7), 1305–1312 (2011).
34. L. N. Thibos, X. Hong, A. Bradley, and R. A. Applegate, "Accuracy and precision of objective refraction from wavefront aberrations," J. Vis. **4**(4), 329–351 (2004) doi:10.1167/4.4.9.
35. M. O. Mello, Jr., I. U. Scott, W. E. Smiddy, H. W. Flynn, Jr., and W. Feuer, "Surgical management and outcomes of dislocated intraocular lenses," Ophthalmology **107**(1), 62–67 (2000).
36. A. Galor, M. Gonzalez, D. Goldman, and T. P. O'Brien, "Intraocular lens exchange surgery in dissatisfied patients with refractive intraocular lenses," J. Cataract Refract. Surg. **35**(10), 1706–1710 (2009).
37. J. M. Artigas, J. L. Menezo, C. Peris, A. Felipe, and M. Díaz-Llopis, "Image quality with multifocal intraocular lenses and the effect of pupil size: comparison of refractive and hybrid refractive-diffractive designs," J. Cataract Refract. Surg. **33**(12), 2111–2117 (2007).
38. C. Dorronsoro, J. R. Alonso-Sanz, D. Pascual, A. Radhakrishnan, M. Velasco-OCana, P. Perez-Merino, and S. Marcos, "Visual performance and perception with bifocal and trifocal presbyopia corrections simulated using a hand-held simultaneous vision device," Invest. Ophthalmol. Vis. Sci. **56**, 4306 (2015).
39. P. de Gracia, C. Dorronsoro, Á. Sánchez-González, L. Sawides, and S. Marcos, "Experimental simulation of simultaneous vision," Invest. Ophthalmol. Vis. Sci. **54**(1), 415–422 (2013).
40. J. J. Esteve-Taboada, A. J. Del Águila-Carrasco, I. Marín-Franch, P. Bernal-Molina, R. Montés-Micó, and N. López-Gil, "Opto-mechanical artificial eye with accommodative ability," Opt. Express **23**(15), 19396–19404 (2015).
41. A. Bradley, P. S. Kollbaum, and L. N. Thibos, "Multifocal correction providing improved quality of vision," U.S. patent US8894203 B2 (November 25, 2014).
42. J. Porter, A. Guirao, I. G. Cox, and D. R. Williams, "Monochromatic aberrations of the human eye in a large population," J. Opt. Soc. Am. A **18**(8), 1793–1803 (2001).
43. A. P. Ginsburg, "Contrast sensitivity: determining the visual quality and function of cataract, intraocular lenses and refractive surgery," Curr. Opin. Ophthalmol. **17**(1), 19–26 (2006).
44. J. Carballo-Alvarez, J. M. Vazquez-Molini, J. C. Sanz-Fernandez, J. Garcia-Bella, V. Polo, J. García-Feijoo, and J. M. Martinez-de-la-Casa, "Visual outcomes after bilateral trifocal diffractive intraocular lens implantation," BMC Ophthalmol. **15**(1), 26 (2015).

1. Introduction

Accommodation is an important mechanism of the young eye to bring nearby objects into focus and creating sharp and clear images at the retina. As the eye ages, however, its accommodation ability declines [1–3] until it is lost almost completely at the early fifties, when the eye is already said to be presbyopic. The most obvious consequence of presbyopia

Biomedical Optics EXPRESS

is blurred near vision, making hard to accomplish near tasks (e.g. reading the newspaper). Nowadays, there is a wide range of available tools for counteracting presbyopia symptoms [1,4,5], based on different strategies, such as ophthalmic lenses, contacts lenses (CLs), intraocular lenses (IOLs), and surgical techniques. We can distinguish two basic strategies for presbyopia treatment: simultaneous vision and alternating vision.

Simultaneous vision is based on simultaneous projection of images on the retina at the same time [1,4,5]. Each projected image corresponds to a sharp image at a different vergence. Typically, this solution is achieved by multifocal CLs [1,5] or IOLs with refractive [4] or diffractive [4,6] profiles. Success of simultaneous vision relies on the ability of the human brain to select among the superimposed images a primary in-focus image [1], suppressing the blurred out-of-focus image. The drawback of this strategy is that suppression ability varies among individuals [7]; the out-of focus images, if not suppressed, can generate a great amount of blur and reduce the contrast sensitivity [1,4,8]. Monovision [1,4,5], where one eye receives the correction for far vision and the other for near, can be considered as simultaneous vision if the binocular rivalry between the retinal images generates binocular suppression. Large depth-of-focus (DoF) achieved by using a pinhole in a contact lens [9], in a corneal inlay [10] or near the pupil plane [11], also allows for simultaneous vision.

Alternating vision refers to images of objects at different vergences generated at the retina at different times. This is a strategy followed by bifocal, trifocal or progressive ophthalmic lenses [1]. CLs for alternating vision (with two distinct power segments alternating with upward and downward gaze shifts) also exist [1,5]. Accommodative IOLs [12] have been introduced that theoretically can change their power when the ciliary muscle is activated by the accommodation reflex, but their effectiveness is yet to be proven.

Although both types of multifocality are different in essence, their visual effects are identical if alternating vision is produced at a high temporal frequency. For a stimulus to be perceived as stable or smooth and without flickering, it should be presented to the eye at a rate above a threshold known as the critical flicker frequency [13,14], at around 9 Hz at scotopic light levels and 50 Hz at high photopic light levels [15]. According to Bloch's Law [13,14], within sufficiently short time intervals (<100 ms) the visual system makes a temporal summation of brightness so that stimulus intensity and duration are reciprocally proportional to each other. Temporal multiplexing can be used to generate simultaneous vision. It allows for adjusting the proportion of time in far and near vision by direct modulation of light energy distribution between the two foci. Simultaneous vision with temporal multiplexing can be achieved artificially with high-speed optoelectronic devices, such as a tunable focal lens [16]. The practical use of those devices is limited since they are relatively heavy, big, and need a power supply. However, they can be a good way to test visual performance under simulated multifocality in a presbyopic eye prior to IOLs' implantation [17].

Some simultaneous vision designs include manipulation of higher-order aberrations (HOAs), since they have been found to influence the visual performance of subjects with presbyopic solutions [18–20]. For instance, IOLs with negative spherical aberration (SA) aim to compensate the positive SA aberration of a pseudophakic eye [21]. However, the presence of negative SA in IOLs can generate difficulties in vision clarity if they get displaced [22,23]. On the other hand, the presence of a certain amount of SA in the eye may also be useful to increase DoF [24,25]. Within this frame, it would be desirable to explore the possibility of testing multifocality in the presence of certain values of HOAs (e.g. SA), and for instance, explore the possibility of inducing different amounts of SA for the far and near vision, mimicking the young eye where usually SA is positive for the relaxed state and negative for accommodation states larger than 2-3 D [26].

In this study, we used temporal multiplexing with a deformable mirror (DM) to generate simultaneous vision and to assess the through-focus optical performance (in terms of contrast) of different designs with equal and unequal distribution of energy in each focus. We also generated a toric equal energy design by inducing astigmatism and explored the effect of SA

Biomedical Optics EXPRESS

in far and near foci. Finally, we explored the effect of SA on a pseudophakic 60-year-old eye. Although our findings are based on simulated conditions, the methodology can be applied to assess visual performance with simultaneous vision designs in real subjects.

2. Methods

2.1 Experimental set-up

A diagram of the AO visual simulator (MurciAO) used in this study is shown in Fig. 1. The system has four principal components: a 40 × 32 lenslets Shack-Hartmann aberrometer (HASO4 First, Imagine Eyes, Orsay, France), an electromagnetic DM (Mirao 52e, Imagine Eyes, Orsay, France) with a membrane of 52 piezoelectric actuators, a Badal system built on two flat mirrors mounted on a monitorized stage (PLS-85, PI miCos), and an 800 × 600 black-and-white microdisplay (eMAGIN, USA). For the experiments conducted in this study, a digital camera (E-M5, Olympus, Tokyo, Japan) was placed in the entrance pupil (5-mm) of the AO system, acting as an artificial eye. A He-Ne laser of 633 nm was used to measure and correct the aberrations of the system.

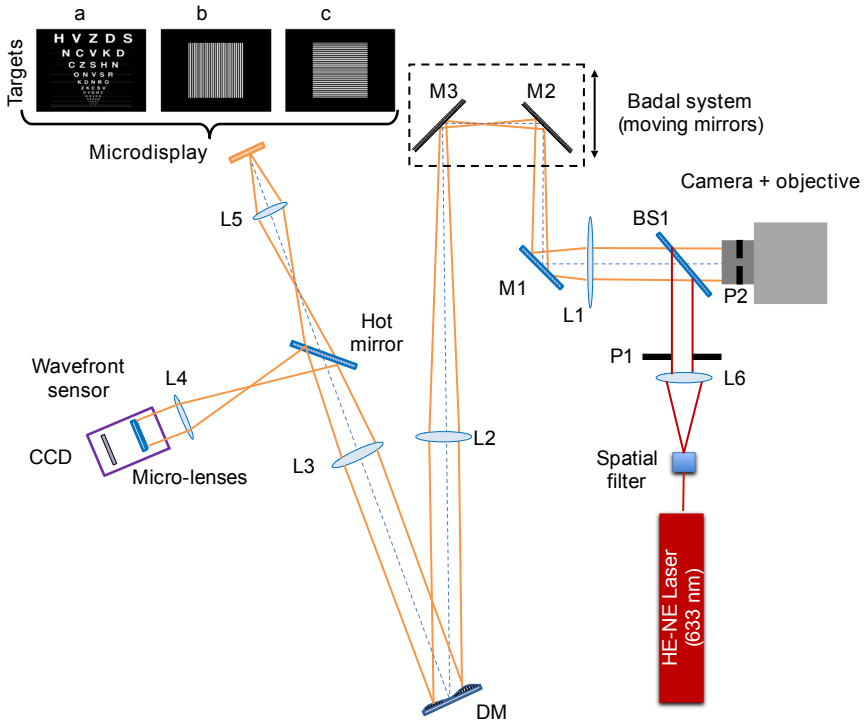

Fig. 1. Schematic diagram of the AO system (MurciAO). Lenses L1, L2, L3, and L5 are achromatic doublets; lenses L4 and L6 are singlets; M1, M2, and M3 are flat mirrors; P1 is an artificial pupil; P2 is the camera stop; and BS1 is a pellicle beam splitter. Targets on the left side are (a) an acuity chart, (b) a vertical square grating, and (c) a horizontal square grating described in Section 2.2.

Simultaneous vision patterns were generated by continuously changing the shape of the DM between two vergences: one for far focus at 0 D and one for near focus at −2.5 D, a simultaneous vision design for subjects of more than 55 years of age with near zero amplitude of accommodation [27]. The residual root mean square was always below 0.1 µm for an 8.2-mm pupil diameter. To avoid flickering effects, the frequency at which the mirror changed position was 50 Hz (i.e. 20 ms) [13,14]. We created two rotationally symmetrical designs for bifocal simultaneous vision: one in which the DM stayed 50% of the time in each foci and

Biomedical Optics EXPRESS

other in which the mirror stayed 60% of the time in the far focus and 40% in the near focus. These designs correspond, respectively, to the equal energy design (50/50) and the unequal energy design (60/40). Because the DM needs 5 ms to change its shape, the effective time the mirror was still in each vergence was 5 ms for the equal energy (50/50) design and 7 ms and 3 ms for the unequal (60/40) energy design. Figure 2 shows digital photographs of the visual acuity charts at different vergences for three different simultaneous vision designs generated with the AO system. The supplemental video (and see a still image in Fig. 3) demonstrates the simultaneous vision generated with the AO system. A Sloan letter was presented as target and bifocality was generated as the DM changing shape between 0 D to −2.5 D of vergence at 50 Hz. Simultaneously, the Badal system moved at constant speed from + 0.5 D to −3.5 D. The two vergences where the target is seen with highest contrasts correspond to the positions of the Badal system for which the stimulus vergence was 0 and −2.5 D.

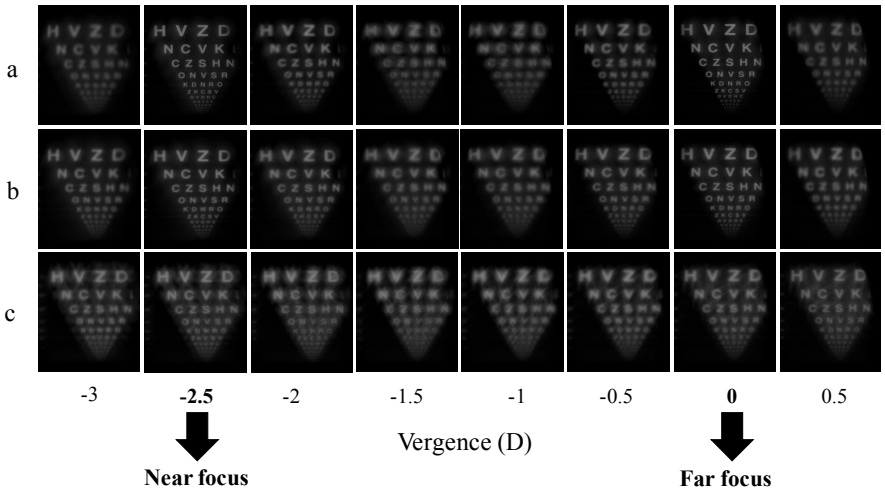

Fig. 2. Through-focus photographic images of a visual acuity chart for three bifocal designs: (a) equal energy design; (b) equal energy design with negative SA at the far focus and positive SA at the near focus; (c) equal-energy design with corneal HOAs (up to 7th order). Arrows indicate the far and near foci.

Fig. 3. Visualization 1 shows a through-focus video of a Sloan E when simulating a bifocal equal energy (50/50) design, when vergence changed from 0.5 D to −3.5 D at a temporal frequency of 50 Hz.

Table 1 below summarizes all the designs generated in this study.

Biomedical Optics EXPRESS

Table 1. Summary of the simultaneous vision designs generated with AO. F reads for far focus and N for near focus. Note that the SA values herein are given for a 5-mm pupil diameter.

Design	Energy Distribution (%)[a]	Comments[a,b]
Equal-energy bifocal	50 (F) / 50 (N)	
Unequal-energy Bifocal	60 (F) / 40 (N)	
Bifocal Toric	50 (F) / 50 (N)	1 D of astigmatism at 0°
Bifocal with SA	50 (F) / 50 (N)	+ 0.1 µm (F) / + 0.1 µm (N) –0.1 µm (F) / –0.1 µm (N) –0.1 µm (F) / + 0.1 µm (N) + 0.1 µm (F) / –0.1 µm (N)
Bifocal + Corneal HOAs	50 (F) / 50 (N)	HOAs from a model cornea of 60 years of age
Bifocal with SA + Corneal HOAs	50 (F) / 50 (N)	–0.1 µm (F) / –0.1 µm (N) and HOAs from a model cornea of 60 years of age

[a]N means near focus and F means far focus

[b]SA values are for 5-mm pupil

For the equal-energy design, we explored toricity and SA effects on lens design. Astigmatism and SA were added using the DM (Fig. 1). First, we explored a toric bifocal design (a non-rotationally symmetrical design) with −1.0 D of astigmatism at 0°. We also tested different combinations of SA (a rotationally symmetrical design) for the far and near foci to evaluate their effect on the DoF (see Table 1). The value was chosen following the amounts of negative SA that monofocal IOLs have; around −0.2 µm for a 6-mm pupil size [28] rescaled to a 5-mm pupil.

Finally, we assessed the effect of corneal HOAs of a 60-year-old eye to the bifocal 50/50 energy IOL design. The goal of this simulation was to know if the aberrations generated by the patient's cornea had an impact on the in vitro through-focus curve of a multifocal IOLs. For that purpose, up to 7th order corneal HOAs (SA + 0.19 µm for a pupil size of 5 mm) were obtained from an aging model cornea [30]. These corneal HOAs were added to the bifocal design with the DM to simulate:

a) a pseudophakic eye with a bifocal IOL of zero SA,

b) a pseudophakic eye with a bifocal IOL and −0.1 µm of SA (induced in each foci) to compensate part of the positive corneal SA of the aphakic eye [28].

2.2 Measurements

Through-focus curves were recorded for each of the simulated simultaneous vision designs. A step-by-step electric motor was used to change the optical path length between L1 and L2 (Badal system) in steps of 0.125 D. The range of the through-focus curves was from + 0.5 D to −3 D, except for the toric design, for which the range was from + 0.5 D to −4 D due to the astigmatic power. At each step, three different targets were successively projected on the microdisplay (luminance level at 260 cd/m^2) and an image of each target was captured with

Biomedical Optics EXPRESS

the camera while the mirror was changing its shape between the two vergences. The targets are shown in Fig. 1. They were an acuity chart, a vertical square grating, and a horizontal square grating. The gratings had a spatial frequency of 15 cpd, which is the spatial frequency typically used to evaluate in vitro optical quality of IOLs [31,32]. The size of each image registered with the camera was 4608x3456 pixels with a pixel size of 3.74 μm. The focal length of the camera objective used was 50 μm, therefore every pixel subtended 15.4 arcsec. The exposure time of the camera was set at 0.16 s to match the temporal summation properties of the human eye [13].

In all measurements, we proceeded as follows. First, reference images were taken for each of the three targets in Fig. 1 with the mirror still and all the aberrations of the system corrected. Then, three through-focus curves were obtained for each target. After each through-focus curve was obtained, the aberrations of the system were corrected again and new reference images were taken prior measuring the next through-focus curve for the next simulated simultaneous vision design.

2.3 Data analysis

Normalized cross-correlation coefficients [33] were calculated for the acuity chart and Michelson contrast was calculated for the gratings, at each vergence of the through-focus curve. For the calculations, customized software developed in Matlab (Mathworks, Inc., Natic, MA) was used. Due to a small vignetting effect from the system's optics, a central area (150 × 200 pixels) of the images was chosen for the calculations. The normalized cross-correlation indicates the similarity between the reference image and the rest of the images in the through-focus. Contrast was normalized by dividing the contrast value of each image with the contrast value of the reference image, which was always greater than 0.9. For the rotationally symmetrical designs, where only defocus and SA were modified, the through-focus curve of the horizontal and the vertical grating were averaged.

Experimental contrast results were compared against computer simulations generated with the Fourier Optics Calculator [34] for MatLab (Mathworks, Inc., Natic, MA). The selected pupil used was 5 mm, as the experimental one, and the wavelength was 550 nm.

3. Results

Figure 4 shows the experimental through-focus curves (in black) of the normalized Michelson contrast (upper panel) and of the normalized cross-correlation (lower panel) for the equal-energy, unequal-energy, and toric designs. For normalized Michelson contrast, theoretical through-focus curves are also shown in gray. Theoretical curves were not included for the cross-correlation values, since they are less sensitive to a contrast reduction caused by a secondary, out-of-focus image. For the toric design, the experimental cross-correlation peaks (marked with arrows in the lower-right panel) are located at 0 D and at −1.0 D for far vision and at −2.5 D and −3.5 D for near vision. The theoretical through-focus curves showed greater peaks than the experimental ones although, for the intermediate distance, they showed deeper valleys than the experimental curves.

Biomedical Optics EXPRESS

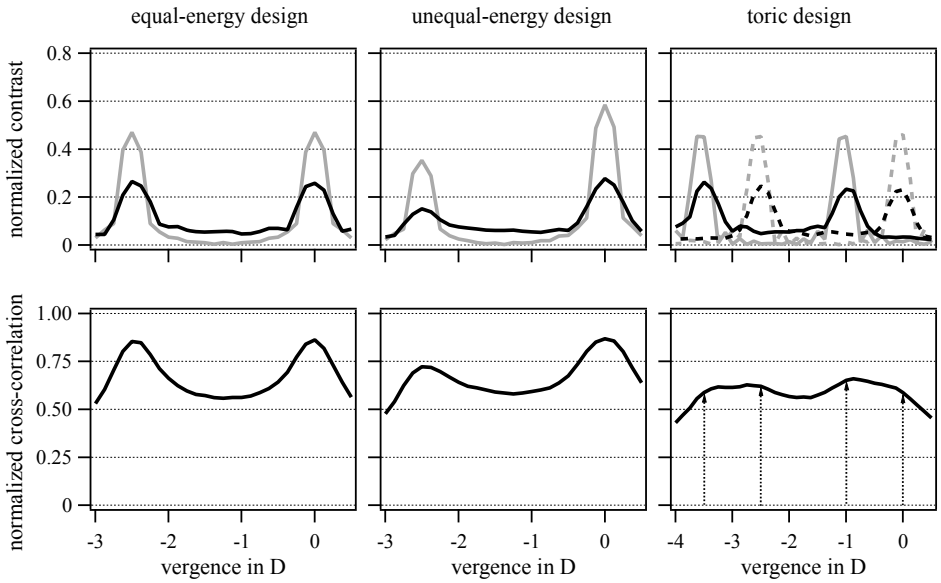

Fig. 4. Experimental (black) and simulated (grey) through-focus curves for simultaneous vision designs: equal-energy (50/50) design (left), unequal-energy (60/40) design (center), and equal energy (50/50) toric design with 1.0 D of astigmatism at 0° (right). The dashed lines in the upper-right panel are the experimental and theoretical curves for the meridian with no astigmatic power whereas the continuous lines correspond to the meridian that has the astigmatism. The black arrows in the lower-right panel indicate the peaks for far and near vision of the toric design. Notice that the through-focus curves for the toric design are 1.0 D wider than for the rest.

Figure 5 shows experimental and simulated through-focus curves for normalized Michelson contrast for the four combinations of SA.

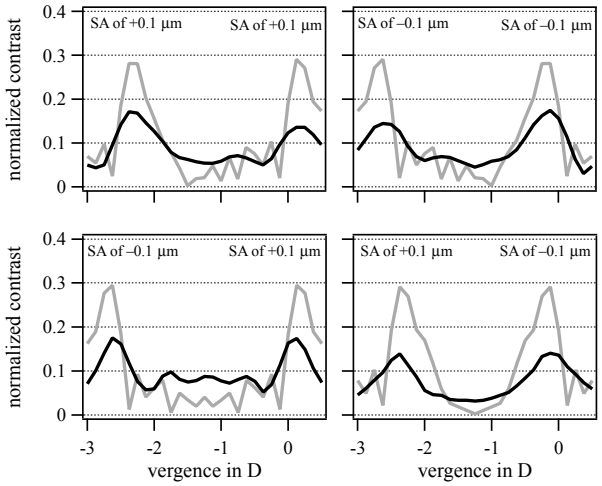

Fig. 5. Experimental (black) and simulated (grey) through-focus curves of the normalized contrast for different combinations of SA in near and far foci. The upper panel shows through-focus curves when (left) positive SA was added to both foci and (right) negative SA was added to both foci. Lower panel shows through-focus when (left) positive SA was added to far focus and negative SA to near focus and (right) negative SA was added to far focus and positive SA to near focus. Notice that the y-axis has been rescaled for visualization purposes.

Biomedical Optics EXPRESS

The addition of SA to the bifocal equal-energy design decreased the optical quality of the peaks but increased their width. Bumps were evident at intermediate vergences but the optical quality did not increase. Adding positive SA to both near and far foci shifted the two peaks of the curve to the right by 0.125 D. Adding negative SA had the opposite effect, shifting the curve to the left by the same amount. The addition of positive SA to the far focus and negative SA to the near focus separated the peaks from each other by 0.25 D, whereas addition of negative SA to the far focus and positive SA to the near focus brought the peaks closer together by the same amount. Figure 6 shows the same data as in Fig. 5 but for the normalized cross-correlation.

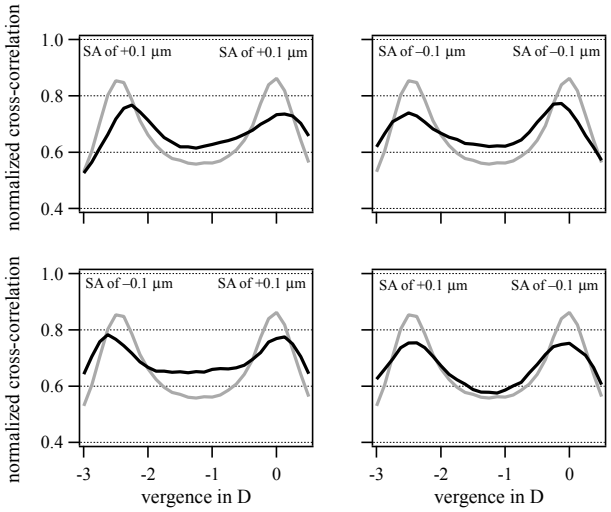

Fig. 6. Simulated (grey) through-focus curves of the normalized cross-correlation for different combinations of SA in near and far foci. For comparison purposes, the cross-correlation curve of the equal-energy bifocal (black curve) is included in each panel. The upper panel shows through-focus curves when (left) positive SA was added to both foci and (right) negative SA was added to both foci. Lower panel shows through-focus when (left) positive SA was added to far focus and negative SA to near focus and (right) negative SA was added to far focus and positive SA to near focus.

As expected, for each combination of SA, the through-focus curves for normalized cross-correlation showed the same behavior as the through-focus curves for normalized Michelson contrast: a decrement in optical quality in peaks, an increase at intermediate vergences, and same shifts in peaks (to the right for positive SA and to the left for negative SA).

Figure 7 shows the experimental through-focus curves for comparing the effects of partially compensating (gray curves) or not (black curves) the SA of a normal 60-year-old pseudophakic eye with an ideal equal-energy bifocal lens.

Biomedical Optics EXPRESS

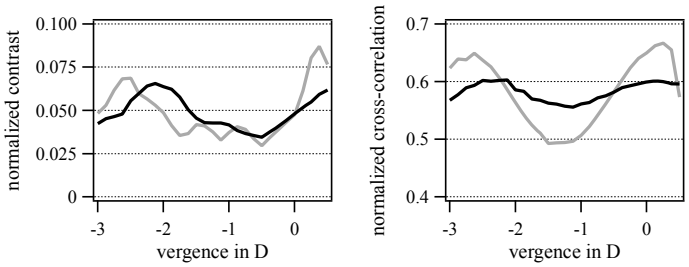

Fig. 7. Through-focus curves for normalized Michelson contrast (left) and normalized cross-correlation (right) for a 60-year-old pseudophakic eye wearing an ideal equal-energy bifocal lens without SA (black) and with negative SA (gray) in both foci (–0.1 μm) for partially compensating the positive SA of the model cornea (+ 0.19 μm). Notice that the y-axis has been rescaled for visualization purposes.

Note the changes between black and gray lines in Fig. 7. The optical quality of the peaks dropped significantly when the corneal HOAs were added to the equal-energy bifocal lens. Additionally, they were also displaced to the right by 0.325 D for the near focus and by 0.5 D for the far focus. The addition of negative SA slightly improved the quality at the peaks and restored their placement (near peak placed at −2.5 D and far peak placed at 0.125 D).

4. Discussion

We propose a method based on temporal multiplexing simultaneous vision to simulate the visual optical effects of multifocal designs using AO technology. This methodology allows us to test the effects of not only defocus but also other aberrations such as astigmatism in toric designs or spherical aberration in most actual multifocal CLs and IOLs designs. It can be used to obtain a more realistic through-focus curve of multifocal solutions (CLs, IOLs) in a particular eye and also for evaluating the interactions between multifocal IOLs designs and corneal aberrations prior surgery.

This methodology can be applied for performing measurements in real subjects as long as the frequency at which the DM changes shape is equal or greater than 50 Hz, to prevent flickering effect [13,14]. Although we did not assess subjective through-focus curves with real eyes, we observed the stimulus with our own eye (looking through the system), to ensure that there was no flickering, before conducting the experiments described here. We noted that, when the eye was not perfectly aligned with the system, the out-of-focus (ghost) image appeared a little bit shifted with respect to the in-focus image (vergence of 0 D). Indeed, this shift is also experienced by pseudophakic eyes when having an IOL that is not well centered [35,36].

The peaks and valleys in the experimental through-focus curves for Michelson contrast were consistent with those for cross-correlation (see Figs. 4 to 7). In addition, theoretical through-focus curves for Michelson contrast were consistent with our experimental measurements (see Figs. 4 and 5). Yet, the peaks for the theoretical curves were systematically greater than the ones for the experimental curves. The bumps were more evident at the middle points for the theoretical curves than for the experimental ones. These differences between experimental and theoretical curves may be due to a smoothing effect generated as a consequence of the amount of time the mirror takes to change shape, as illustrated through the simulations shown in Fig. 8. In the calculation of the theoretical curves, we implicitly assume that the mirror can move instantly from near to far focus (dotted gray curves in Fig. 8), but in practice the mirror needed 4 ms to 5 ms (solid gray curve in Fig. 8). This technical limitation becomes increasingly more acute as we increase the number of foci in simulate simultaneous vision (i.e. a trifocal IOL).

Biomedical Optics EXPRESS

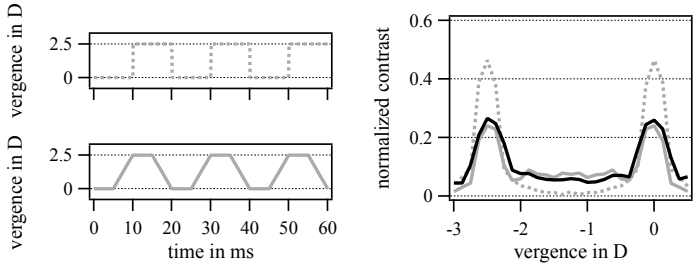

Fig. 8. Upper left panel shows the behavior of the mirror if it changed shape instantly. Bottom left panel shows a more realistic (continuous) change of the defocus. Right panel shows simulated through-focus curves for both situations on the left (dotted gray line corresponds to the top profile change; gray solid line corresponds to the bottom profile change), and also the real through-focus curve (solid black line) for comparison purposes.

Another limitation of the methodology proposed is to reproduce the scatter effects of diffractive optics. Moreover, our methodology cannot assess the effects of diffraction caused by real IOLs with different power zones [6,37]. For instance, a bifocal IOL with radial center-near design has two power zones which correspond to far and near vision, respectively. Thus, the near-focus image is formed by light passing through the central circular area, whereas the far-focus image is formed by light passing through the peripheral annulus. In our experiment, however, both images were formed from light passing through the whole circular pupil at different times. Figure 9 illustrates, after computational simulations, the differences respect to our approach of having two different zones, both with the same area, one for the far and one for the near focus, on normalized contrast. The differences are rather small, although the peak of the far focus decreases in the two-zone IOL simulations. For a center-distance design, the curve simply flips horizontally, that is, the lower peak would be at −2.5 D of vergence.

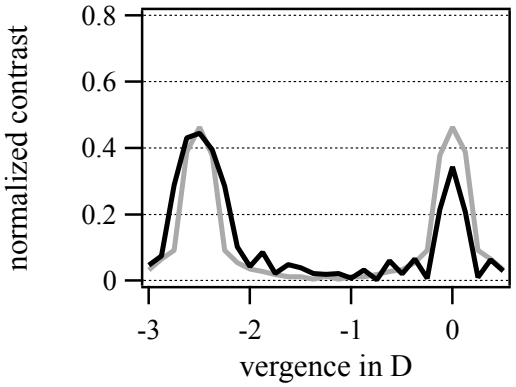

Fig. 9. Computed simulations of the through-focus of a center-near bifocal IOL (black) and an equal-energy bifocal design, where both images share the whole pupil (grey).

Simulated simultaneous vision can also be achieved with a simpler, portable optical system with a tunable lens [38] or with two optical paths [39]. Although a tunable lens is a good option for experiments that involve temporal multiplexing, care should be taken when using it in a vertical position since its membrane can be deformed by the action of gravity, inducing aberrations such as coma [16,40]. A system, as the one shown in Fig. 1, allows us also to simulate the visual effects of bifocal toric designs (see in Fig. 4), as well as designs with different combinations of SA (see Figs. 5 and 6). We tested whether the inclusion of negative SA in for far focus and positive for near focus reduced the visibility of the defocused images (hence improving the image quality) [41]. We tested that combination in an equal-energy design with four combinations of SA (see Figs. 5 and 6). As it can be noticed in the

Biomedical Optics EXPRESS

lower-right panel of Fig. 5, the DoF of the peaks increased with respect to the equal-energy pattern with no SA. The opposite condition (in Fig. 5, lower-left panel) enhanced the intermediate image quality.

Ocular SA varies significantly among older population [24,42], therefore, the through-focus curve depends on the subject and the selected IOL's SA. As an example, the simulations with a pseudophakic 60-year-old eye implanted with an IOL with and without negative SA (Fig. 7), showed how much the corneal aberrations may affect the quality of a bifocal design and the benefit of adding negative SA. However, the quality of the through-focus curves decreased dramatically in both cases. Nevertheless, we should keep in mind that our contrast results are based in gratings with only one spatial frequency while in typical clinical practice, several spatial frequencies are normally used [43].

In conclusion, a fast AO system can be a powerful tool for exploring different aspects of simultaneous vision. Besides the tests performed in the present work, multiple designs and combinations can be tested including trifocal lenses [4,31,32,44] and apodized lenses [6]. Although the results of this study are based on objective measurements and computer simulations, they can be the basis for a series of experiments in subjects to test their visual performance with different multifocal designs.

Funding

This study was supported by the AGEYE project (608049), the Marie Curie Initial Training Network program (FP7-PEOPLE-2013-ITN), granted by the European Commission, Brussels, Belgium and by an Atracció de Talent (University of Valencia) research scholarship granted to Antonio J. Del Águila-Carrasco (UV-INV-PREDOC14-179135).

Acknowledgments

We thank Rafael Navarro for sharing the corneal aberrations with us.